DNA Double-Strand Breaks Form in Bystander Cells after Microbeam Irradiation of Three-dimensional Human Tissue Models

Olga A. Sedelnikova,[1] Asako Nakamura,[1] Olga Kovalchuk,[2] Igor Koturbash,[2] Stephen A. Mitchell,[3] Stephen A. Marino,[3] David J. Brenner,[3] and William M. Bonner[1]

[1]Laboratory of Molecular Pharmacology, Center for Cancer Research, National Cancer Institute, NIH, Bethesda, Maryland; [2]Department of Biological Sciences, University of Lethbridge, Lethbridge, Alberta, Canada; and [3]Radiological Research Accelerator Facility, Center for Radiological Research, College of Physicians and Surgeons, Columbia University, New York, New York

Abstract

The "radiation-induced bystander effect," in which irradiated cells can induce genomic instability in unirradiated neighboring cells, has important implications for cancer radiotherapy and diagnostic radiology as well as for human health in general. Although the mechanisms of this effect remain to be elucidated, we reported previously that DNA double-strand breaks (DSBs), directly measured by γ-H2AX focus formation assay, are induced in bystander cultured cells. To overcome the deficiencies of cultured cell studies, we examined α-particle microbeam irradiation–induced bystander effects in human tissue models, which preserve the three-dimensional geometric arrangement and communication of cells present in tissues *in vivo*. In marked contrast to DNA DSB dynamics in irradiated cells, in which maximal DSB formation is seen 30 min after irradiation, the incidence of DSBs in bystander cells reached a maximum by 12 to 48 h after irradiation, gradually decreasing over the 7-day time course. At the maxima, 40% to 60% of bystander cells were affected, a 4- to 6-fold increase over controls. These increases in bystander DSB formation were followed by increased levels of apoptosis and micronucleus formation, by loss of nuclear DNA methylation, and by an increased fraction of senescent cells. These findings show the involvement of DNA DSBs in tissue bystander responses and support the notion that bystander DNA DSBs are precursors to widespread downstream effects in human tissues. Bystander cells exhibiting postirradiation signs of genomic instability may be more prone than unaffected cells to become cancerous. Thus, this study points to the importance of considering the indirect biological effects of radiation in cancer risk assessment. [Cancer Res 2007; 67(9):4295–302]

Introduction

When unirradiated cells are cocultured with irradiated ones or grown in the medium from irradiated cells, they exhibit many of the same responses as hit cells. This "radiation-induced bystander effect" has become the focus of extensive research (reviewed in refs. 1–3). Current data link radiation-induced bystander effects with a wide range of end points, all of which may result from genomic instability (4–6). These end points encompass altered clonogenic survival, changed frequency of gene mutations, induction of apoptosis and micronuclei, altered expression of stress-related genes, elevated frequencies of malignant transformation of mammalian cells *in vitro* (4, 7), and various epigenetic changes (8, 9).

Studies of cells deficient in DNA double-strand breaks (DSBs) and base excision repair suggested that DSBs rather than base damage play a role in the bystander response (10). Our group and others reported direct evidence that DNA DSBs, measured by γ-H2AX focus formation (reviewed in refs. 11, 12), are a part of the cellular bystander response (13–15).

Most studies on bystander effects have examined long-term effects either in conventional cell cultures, which lack the geometric arrangement and cell-cell communication present in tissues, or in various models of human tissues, including urothelial tissue explants (16–19), spheroids (20), and reconstructed human skin models (21). In contrast, our interests have been to identify short-term cellular responses that may be the progenitors of these longer-term manifestations. Our studies in primary cell cultures showed that whereas γ-H2AX foci formed by 30 min after exposure and disappeared over 18 h in irradiated cells, bystander focal formation was maximal at 18 h after irradiation and remained so for up to 48 h after irradiation. Colocalization of γ-H2AX foci in bystander cells with DSB repair proteins confirmed that these foci are sites of DSB repair and suggested that these breaks may be responsible for other downstream bystander effects (13).

Our present study examines the formation and resolution of DNA DSBs in two artificial human tissue models, airway and full thickness skin. The models reconstruct normal tissue structure and preserve *in vivo* differentiation, including the presence of gap junctions, metabolic patterns, and the release of appropriate cytokines (22, 23). These three-dimensional tissue models permit the many damaging and protective effects involved in the bystander response (reviewed in ref. 24), to be studied simultaneously in the same tissue sample *in situ* and over longer times.

After irradiating a thin plane of cells through the tissue with an α-particle microbeam, we analyzed a variety of biological end points in bystander cells as a function of distance (up to 2.5 mm away from the irradiated cell plane) and postexposure time (0 h–7 days). Bystander tissues exhibited an initial increase in DNA DSBs, as well as longer-term increases in apoptosis and micronucleus formation, DNA hypomethylation, persistent growth arrest, increased fractions of senescence-associated β-galactosidase (SA-β-gal)–positive cells, and other phenotypic characteristics of cells undergoing senescence. These findings support the notion that bystander DNA DSB formation initiates the long-term involvement of unexposed tissues surrounding exposed areas in the irradiation-induced bystander response.

Requests for reprints: Olga A. Sedelnikova, Laboratory of Molecular Pharmacology, Center for Cancer Research, National Cancer Institute, NIH, Room 5050, Building 37, 9000 Rockville Pike, Bethesda, MD 20892. Phone: 301-402-3649; Fax: 301-402-0752; E-mail: sedelnio@mail.nih.gov.

doi:10.1158/0008-5472.CAN-06-4442

Materials and Methods

Tissue systems and culture. Normal human three-dimensional artificial tissue systems, EpiAirway (Air-100) and EpiDermFT (EFT-300), were obtained from MatTek (Fig. 1*A*). The tissues are 6 mm in diameter and survive 2 to 3 weeks in culture. The tissues were cultured according to recommended protocols, in Millicell-CM culture inserts (Millipore) with a hydrophilic base membrane, and every 2 days, the culture medium was replaced with fresh serum-free medium. The surfaces of the tissues were exposed to air to stimulate differentiation.

Microbeam irradiation and calculations of delivered dose. To produce direct irradiation damage in spatially defined cells in the three-dimensional tissues and guarantee no direct damage to the rest of the cells in the tissue, a microbeam of 7.0 MeV ^{4}He ions produced by the 5-MV Singletron of the Radiological Research Accelerator Facility (RARAF) of Columbia University (25) was used. The beam size was restricted to a 1 to 2 nuclei width along the line of irradiation.

A single plane of tissues was irradiated from below (Fig. 1*B*) through the 20-μm-thick membrane that forms the base of the culture insert. The insert was positioned in a custom-designed holder attached to a microbeam stage. The ^{4}He ion energy at the surface of the tissue was $\sim$4.6 MeV and the range in tissue was $\sim$31 μm. Because the samples were thicker than the particle range, the linear energy transfer (LET) varied from $\sim$100 keV/μm at the membrane/tissue interface to >200 keV/μm as the ions slowed. The average number of particles for 5 μm of translation ($\sim$1 cell nuclear diameter) was 1.9 with a SD of 4% to 5% and a total spread of approximately $\pm$10%. The statistical uncertainty for the number of particles is 1.6%. For a broad beam irradiation, the dose delivered by 0.076 ion/μm^2 (1.9 particles in a 5 $\times$ 5 μm^2 area) with a LET of 100 keV/μm is 3.2 Gy.

Tissue manipulations and biological end points. After irradiation, each tissue was returned to a multiwell dish filled with fresh medium and incubated at 37°C in a humidified atmosphere with 5% CO_2 for different times. Control tissues went through the same procedure without being irradiated. The tissues were then frozen and sectioned into 5- to 10-μm-thick slices, which were perpendicular to the plane of the irradiated cells (Fig. 1*B*). This allowed separate analysis of tissue sections containing either mixed irradiated and unirradiated cells in central areas of the sections or only unirradiated cells in distal areas located within 2.5 mm of both sides of the irradiated plane. The rest of the frozen tissues were used for genomic DNA isolation.

Several end points were assessed in exposed and/or bystander areas. Control tissues for which the central plane of cells had been mock irradiated were included in all experiments. The low density and complex morphology of the fibroblasts in the tissue sections prevented accurate determination of the levels of micronuclei of proliferating cells, and the amount of genomic DNA isolated from EFT-300 tissues was insufficient for accurate determination of DNA methylation.

Immunocytochemistry and telomere fluorescence *in situ* hybridization. For the γ-H2AX assay, frozen sections were dried, fixed in 2% paraformaldehyde, permeabilized with 1% Triton X-100, and processed for immunostaining with a custom-made anti-γ-H2AX rabbit antibody as described previously (26). For double labeling, anti-γ-H2AX primary antibodies were either rabbit or mouse (Upstate BioTech) with anti-Rad50, (Novus Biologicals), anti-53bp1 (generously provided by Dr. J. Chen, Department of Oncology, Mayo Clinic and Foundation, Rochester, MN), anti–cleaved caspase-3 (Trevigen), or anti–proliferating cell nuclear antigen (PCNA; Santa Cruz Biotechnology). Secondary antibodies labeled with either Alexa 488 or Alexa 546 were from Molecular Probes. For telomere

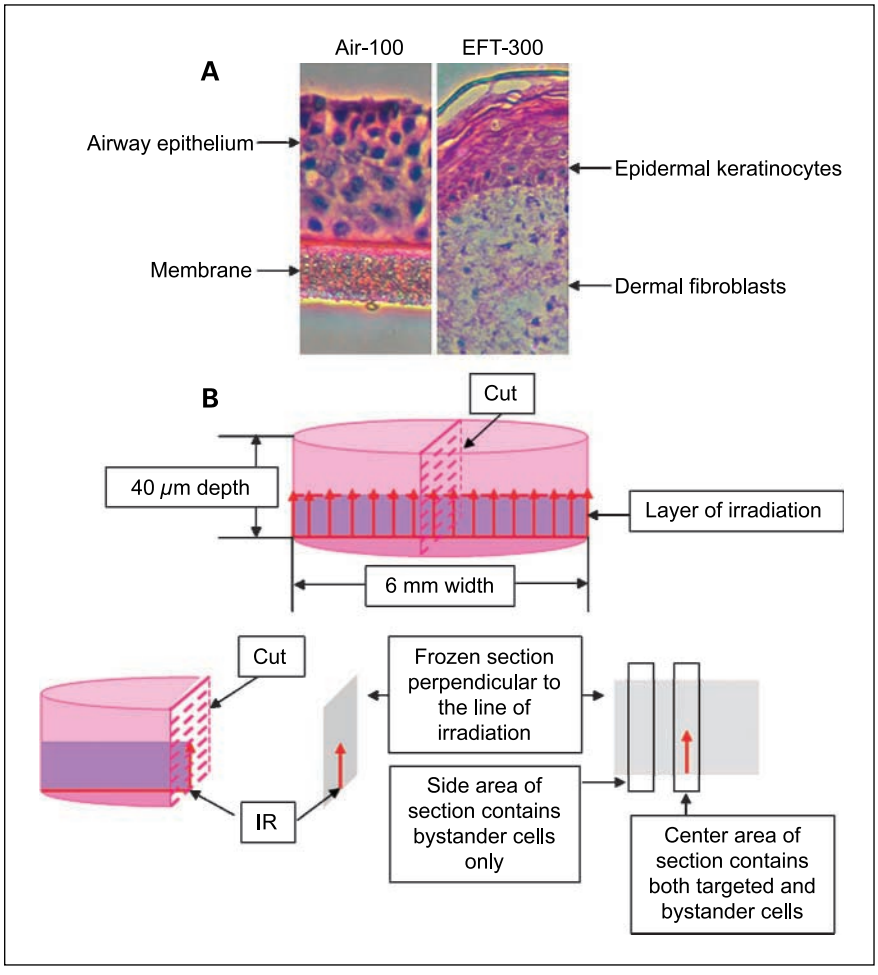

Figure 1. Tissue models and experimental design. *A,* H&E staining of frozen sections of the two human artificial tissue systems, EpiAirway (Air-100), modeling the epithelial tissue of the respiratory tract, and EpiDermFT (EFT-300), which is a "full thickness" skin model consisting of a fibroblast-containing dermal layer and a keratinocyte-containing epidermal layer. *B,* scheme of the irradiation procedure. The tissue consists of a 6-mm diameter cylinder with a height of 40 μm (Air-100) or 300 μm (EFT-300; Air-100 is shown), which is microbeam-irradiated from below through the membrane that forms the base of the culture insert. The tissues were frozen at various times after irradiation and sectioned into slices perpendicular to the irradiated plane of cells. Thus, central areas of the sections contain both irradiated and nonirradiated cells, and side areas contain only unirradiated cells.

fluorescence *in situ* hybridization analysis, frozen sections were processed and hybridized with Cy3-conjugated telomere PNA probes (DakoCytomation) according to the manufacturer's instructions. The nuclei were counterstained with either propidium iodide (PI) or 4′,6-diamidino-2-phenylindole (DAPI). Fluorescent and confocal microscopy was done with a Nikon PCM 2000 (Nikon).

γ-H2AX focus formation assay. γ-H2AX foci were recorded by collapsing 0.5-μm-thick optical Z-sections through the nuclei in a single plane and counted by eye in a blinded fashion in 100 to 260 randomly chosen cells of central and side areas of sections. The results are presented in a "cells with four or more γ-H2AX foci per cell (fpc)" format (≥4 fpc) because we have found previously that using this threshold is optimal for determining the fraction of affected bystander cells (13).

Apoptosis assay. Tissue sections were stained for cleaved caspase-3 and γ-H2AX. Frequencies of cleaved caspase-3–positive cells and these cells associated with γ-H2AX staining relative to all apoptotic cells were recorded for at least 1,000 cells of side section areas.

Micronucleus assay. The analysis was done both in sections stained for γ-H2AX (nuclei were stained with PI) and in sections used for the apoptosis assay (nuclei were stained with DAPI). Both types of nuclear staining revealed similar results. Frequencies of cell nuclei with associated micronuclei, relative to all nuclei, were recorded in at least 1,000 cells of side section areas of Air-100 epithelium and EFT-300 keratinocytes. Frequencies of micronuclei associated with γ-H2AX staining relative to all recorded micronuclei were also found.

SA-β-gal staining. Frozen sections were fixed and stained with the Senescence β-gal staining kit (Cell Signaling Technology) according to the manufacturer's instructions. The samples were photographed with a Nikon Coolpix charge-coupled device camera.

Global genome DNA methylation. Genomic DNA was isolated from frozen Air-100 tissues. A radiolabeled [^{3}H]dCTP extension assay was used to analyze the level of global DNA methylation as described previously (27, 28). In brief, an aliquot of genomic DNA was digested with methylation-sensitive *Hpa*II restriction endonuclease (New England Biolabs). A second DNA aliquot was digested with methylation-insensitive isoschizomer *Msp*I, which cleaves CCGG sites in DNA regardless of CpG methylation status. An aliquot of undigested DNA served as a control. Following the single nucleotide extension reaction, the samples were applied to ion-exchange filters and washed with 0.5 mol/L $NaP0_4$ buffer (pH 7.0), and the dried filters were processed for scintillation counting (Beckman Coulter). The [^{3}H]dCTP incorporation into DNA was expressed as mean disintegrations per minute per microgram DNA after subtraction of the disintegrations per minute incorporation in undigested samples. The absolute percentage of double-stranded unmethylated CCGG sites was calculated by the ratio of incorporation from the *Hpa*II and *Msp*I digests, respectively. The experiment was independently reproduced thrice.

Results

Induction of DSBs in targeted and bystander tissues. Two types of normal human three-dimensional tissue models were subjected to α-particle irradiation focused by a microbeam to a single plane through the tissue block. The EpiAirway tissue system (Air-100) consists of three to four layers of normal, human-derived tracheal/bronchial epithelial cells, which have been cultured to form a highly differentiated tissue ~40 μm thick, which closely resembles the epithelial tissue of the respiratory tract. The EpiDermFT tissue system (EFT-300) is a "full thickness" skin model ~300 μm thick, which has fibroblast-containing dermal and keratinocyte-containing epidermal layers, corresponding to the dermis and epidermis of normal human skin. After incubation for various times, the tissues were frozen and sections perpendicular to the plane of irradiation were taken for assays (Fig. 1*B*).

The levels of γ-H2AX foci were determined in cells at least 1 mm away from the plane of irradiation (distal region, bystander cells; Fig. 2, *blue lines*), as well as in those near the plane (proximal region, a mixture of irradiated and bystander cells; Fig. 2, *red lines*). In contrast to the microbeam protocols in cell cultures, the cells in the three-dimensional tissues were not exposed to any imaging agents, removing concerns about the potential influence of dyes on cellular response to irradiation.

In the Air-100 sections (Fig. 2*A*), the temporal changes in γ-H2AX focal levels differed between the distal and proximal regions. In the distal region, consisting completely of bystander cells, the levels of γ-H2AX foci increased slightly at 0.5 h after irradiation and continued to increase for 2 days after irradiation and then gradually decreased out to 7 days (Fig. 2*A, blue*). At the 2-day maximum, 47% of the distal cell population contained γ-H2AX foci. In contrast, in the proximal region, γ-H2AX focal levels increased for 1 to 2 h, then decreased until 8 h, and increased again to 2 to 5 days after irradiation (Fig. 2*A, red*). This biphasic behavior is consistent with the presence of both hit and bystander cells in this region. Accumulation of 53bp1 and Rad50 in the γ-H2AX foci (data not shown) indicated that DSB repair was ongoing in the bystander cells.

In contrast to the Air-100 system, the EFT-300 "full thickness" skin model contains two cell types, a basal layer of fibroblasts covered with a layer of keratinocytes. The α-particles penetrate into the fibroblast layer but the keratinocytes are out of range. γ-H2AX foci were counted in these two layers separately. In the fibroblast layer, the distal regions of the sections exhibited a measurable increase in the levels of γ-H2AX foci by 2 h after irradiation and a maximal 5.5-fold increase 2 days after irradiation (Fig. 2*B, blue*). As in the Air-100 system, two maxima are present in the proximal regions of the fibroblast sections, reflecting the presence of both irradiated and bystander cells, the first maxima, 3.3-fold at 0.5 h after irradiation, and the second, 4.9-fold at 2 days after irradiation (Fig. 2*B, red*). In the keratinocyte layer, the distal regions of the sections also exhibited measurable increases in γ-H2AX focal incidence by 2 h and a maximal 3.2-fold increase at 12 h after irradiation (Fig. 2*C, blue*). In contrast, the proximal keratinocyte cell population lacks the early 2-h maximum exhibited by the fibroblast layer (Fig. 2*C, red*) but still exhibits measurable increases in focal incidence by 2 h after irradiation with a 3.9-fold for the center areas at 12 h after irradiation. The lack of two maxima in the proximal keratinocyte sections is attributed to the low penetrance of α-particles into tissue (~31 μm); hence, the EFT-300 keratinocytes, completely shielded from the α-particles by the fibroblast layer, were all bystander cells.

Thus, all three types of bystander cells (airway epithelium, dermal fibroblasts, and epidermal keratinocytes) of both tissues (Air-100 and EFT-300) responded with a similar extensive increase in the incidence of DNA DSBs involving 40% to 60% of the cells in the bystander regions. These results indicate that processes affecting genome stability begin in bystander cell populations soon after irradiation of their neighboring population and continue for up to 7 days. In addition, the increased level of γ-H2AX foci in the unirradiated keratinocyte layer is indicative of cross-talk between two cell layers in terms of bystander signaling.

Downstream effects in bystander tissues. We measured the levels of apoptosis, micronuclei, genomic methylation, and senescence in the same or duplicate sections of the same tissue block. Increases of apoptotic cells, measured by the presence of active 18-kDa caspase-3 fragment (29), were apparent in the bystander populations of both irradiated tissue models (Fig. 3*A–C*) at 1 day after irradiation but not at 8 h after irradiation when the levels of γ-H2AX foci had already elevated substantially. For Air-100, the level of apoptosis continued to increase until 4 days after

irradiation, reaching 6.6-fold over controls (Fig. 3*A, gray*). The increases in apoptosis were smaller for the EFT-300 than the Air-100 cells, 2.7-fold for the fibroblasts (Fig. 3*B, gray*) and 2-fold for the keratinocytes (Fig. 3*C, gray*).

Apoptosis initiation followed different kinetics in the two EFT-300 cell types, with an increased incidence in fibroblasts up to 7 days after irradiation, whereas in keratinocytes, and the Air-100 epithelial cells, the incidence was maximal at 1 to 4 days after irradiation and decreased to control values at 7 days after irradiation. This kinetic difference may be due to the fact that the keratinocyte and the Air-100 epithelium layer interface with the medium and air, which may permit apoptotic cell fragments to be eliminated.

Another longer-term result from exposure to irradiation is the formation of micronuclei. The development of micronuclei implies substantial chromosome damage and rearrangement. DNA DSBs are well-known precursors for most irradiation-induced micronuclei (30, 31). In the bystander cells of both Air-100 epithelium and EFT-300 keratinocytes (Fig. 4*A* and *B, gray*), there was an ~2.5-fold increase in micronucleus formation at 2 to 3 days after irradiation, which persisted for 7 days. Again, the presence of increased apoptosis and micronuclei in the unirradiated keratinocyte layer indicates the presence of cross-talk from the fibroblast layer. Belyakov et al. (21) did not find evidence of cross-talk between cell types; however, their criteria of increased apoptosis might not have been sensitive enough to detect the difference.

The apoptotic cells of the bystander tissues contained increased levels of γ-H2AX with increased time after irradiation (Fig. 3*A–C, black*); however, a fraction of apoptotic cells lacked γ-H2AX even at 7 days after irradiation. The involvement of γ-H2AX in apoptosis is unclear. The H2AX-null mouse exhibits apoptosis during spermatogenesis, indicating that apoptosis is independent of the presence of H2AX (32), although another study suggests that it is essential for apoptosis (33).

It also seems that bystander micronuclei may or may not contain γ-H2AX (Fig. 4*A* and *B, black*; Fig. 4*C, white* and *yellow arrows*). This difference may reflect whether the micronucleus formed around whole chromosomes or fragments. The level of micronuclei lacking γ-H2AX remained relatively constant during the time

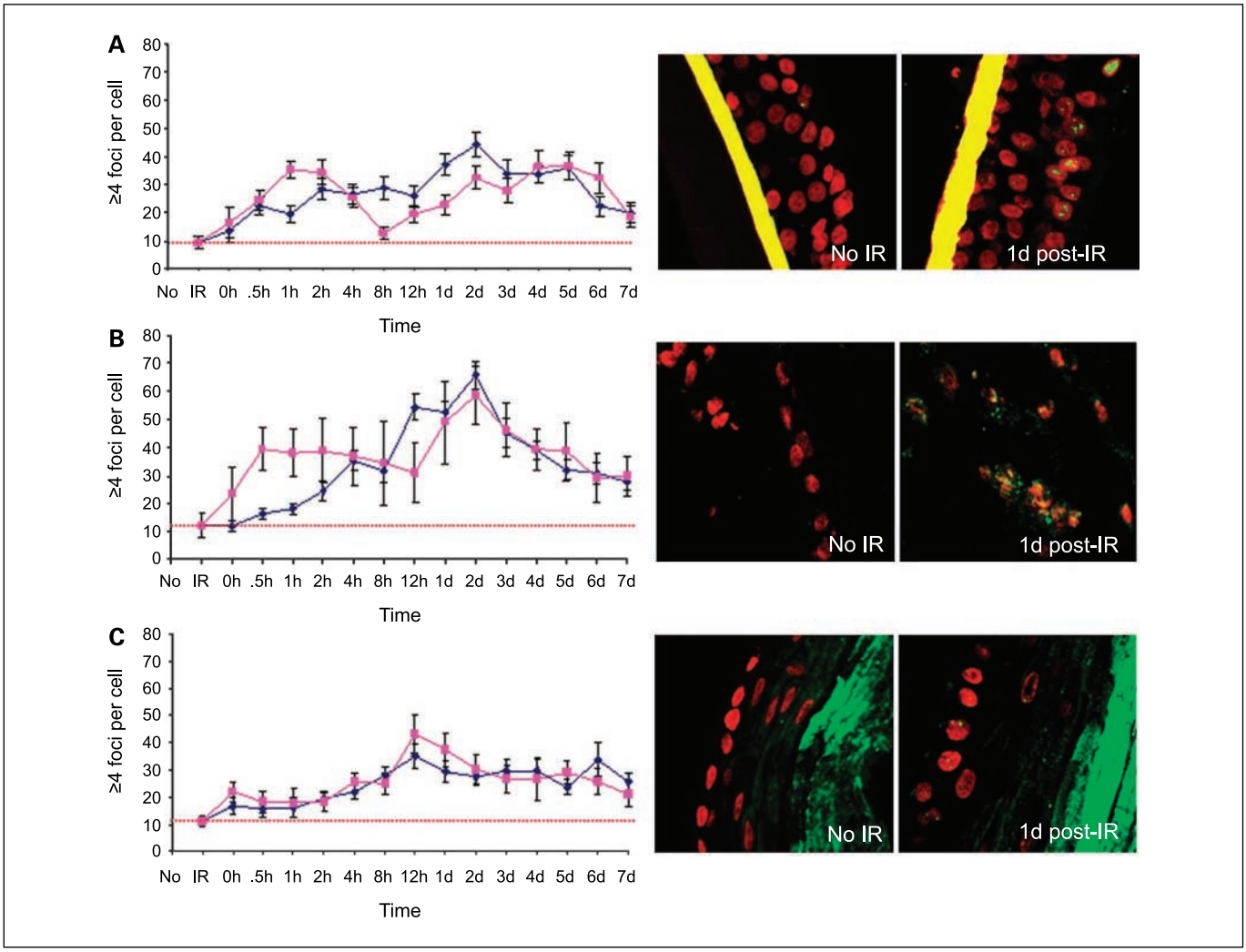

Figure 2. The incidence of γ-H2AX foci in targeted and bystander cells of Air-100 epithelium (*A*), EFT-300 fibroblasts (*B*), and EFT-300 keratinocytes (*C*). γ-H2AX foci were counted in 100 to 260 nuclei per time point in central (mixed irradiated and unirradiated cells; *red*) and side (unirradiated cells; *blue*) areas of the sections. *Dotted lines,* γ-H2AX values in mock-irradiated control tissues. *Points,* ≥4 fpc; *bars,* SDs in percentage and calculated as 100 × square root [(number of cells with 4 or more foci) / (total number of cells counted)]. Representative images show the presence of γ-H2AX foci in corresponding unirradiated and distal bystander tissues 1 d after irradiation. Images are the maximum projections of optical sections showing all recorded foci. γ-H2AX foci are green spots in red cell nuclei counterstained with PI. Magnification, ×40.

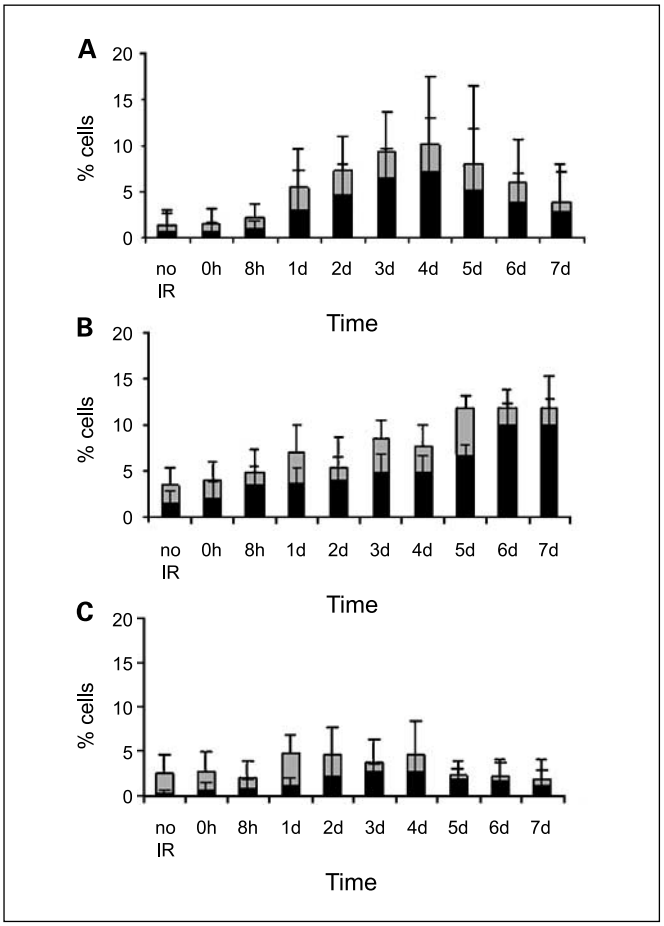

Figure 3. Increase of apoptotic cells in bystander tissues following microbeam irradiation. Cells positive for cleaved caspase-3 (*gray*) and for both cleaved caspase-3 and γ-H2AX (*black*) were recorded at various times after irradiation in Air-100 epithelium (*A*), EFT-300 fibroblasts (*B*), and EFT-300 keratinocytes (*C*). *Columns,* % cells; *bars,* SD.

course, suggesting that the bystander micronuclei formed after irradiation were γ-H2AX positive and originated from broken chromosomes. The presence of γ-H2AX in newly formed micronuclei provides a direct linkage between the formation of bystander DSBs and of micronuclei. In addition, active DNA repair seems to be absent in micronuclei because repair proteins Rad50, Mre11, 53bp1, and Rad17 were not found in the micronuclei,[4] possibly leading to increased numbers of persistent DNA breaks and enhanced γ-H2AX levels.

We examined whether DNA hypomethylation occurs in bystander cells as it is known that a variety of DNA-damaging agents, including irradiation, affect genomic DNA methylation patterns (28, 34–36), perhaps by interfering with the activity of DNA methyltransferases (37, 38). We found that both the targeted and the bystander regions of the Air-100 tissue contained substantial increases in DNA hypomethylation (Fig. 5*A*). The level of unmethylated CCGG sites reached 46% 3 days after irradiation in the bystander regions of the tissue compared with 15% in mock-irradiated controls, a 3-fold change (Fig. 5*A, blue line*). Similarly, in the targeted regions, the percentage of unmethylated CCGG sites peaked at 3 days after irradiation, reaching 70% compared with 24% in controls, a 2.9-fold alteration (Fig. 5*A, red line*). These results show that alterations in global DNA methylation are a part of the bystander response.

Senescence is the irreversible cessation of proliferation of normal cells and is accompanied by increased numbers of DSBs (39), loss of DNA methylation (40), and micronucleus formation (41, 42). Because these three processes are present in bystander cells of irradiated tissues, we examined bystander tissues for several other biomarkers of senescence. A widely accepted biomarker for cellular senescence is the presence of SA-β-gal (43), and increased amounts of SA-β-gal–positive cells were found in all three types of bystander cells in both tissues at 3 to 5 days after irradiation (Fig. 5*B*). As expected, cell proliferation in the senescent bystander AIR-100 and EFT-300 tissues, as measured by the fraction of PCNA-positive cells, was found to be substantially lower than in

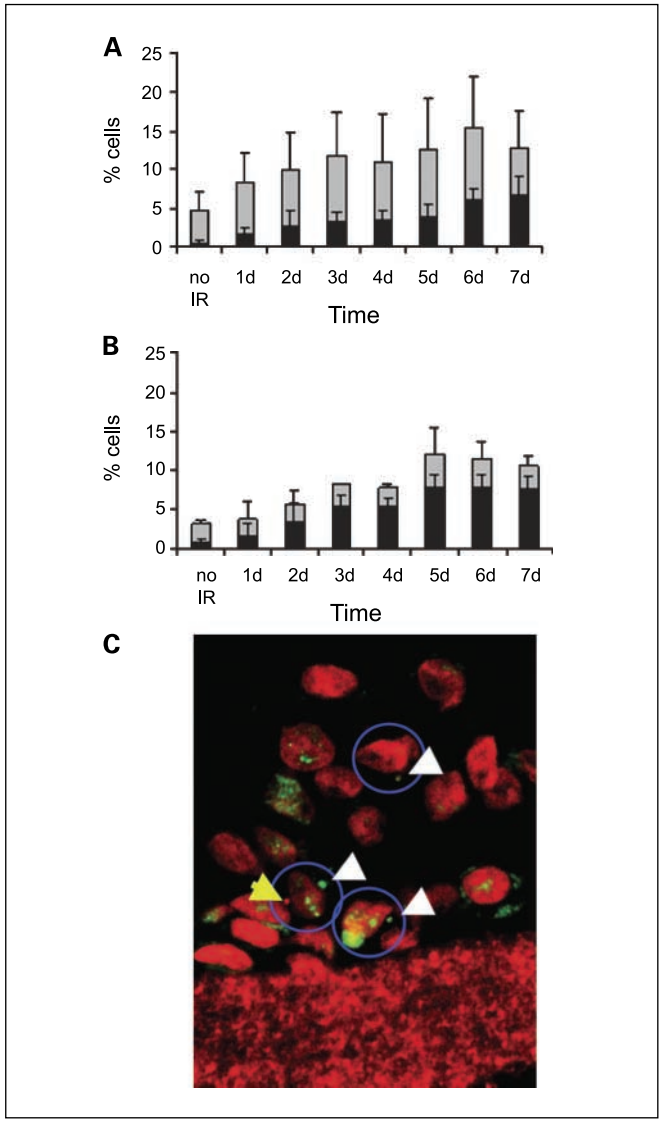

Figure 4. Increase of micronucleated cells in bystander tissues following microbeam irradiation. Cells positive for micronuclei (*gray*) and the micronuclei positive for γ-H2AX (*black*) were recorded at various times after irradiation in Air-100 epithelium (*A*) and EFT-300 keratinocytes (*B*). *Columns,* % cells; *bars,* SD. *C,* micronucleated cells (nuclei and micronuclei are stained with PI; *red*) and micronuclei positive for γ-H2AX (*green*) in bystander tissues of Air-100 epithelium. *Blue outline,* micronucleated cells. *White arrows,* micronuclei positive for γ-H2AX; *yellow arrow,* a micronucleus without γ-H2AX staining.

[4] I. Panyutin, personal communication.

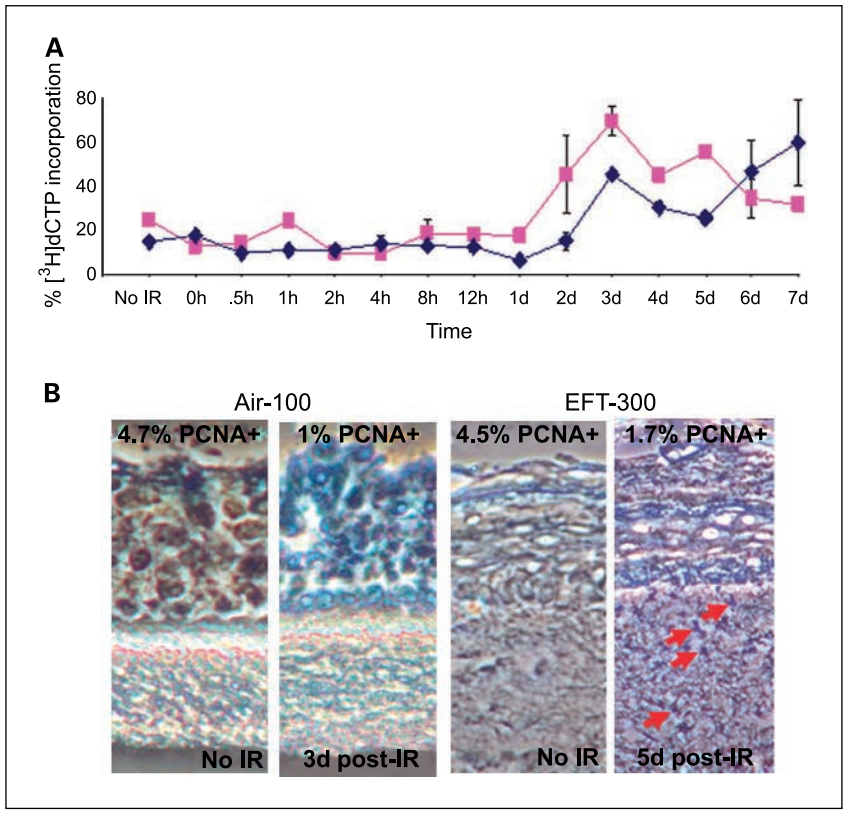

Figure 5. *A,* relative levels of global DNA methylation in targeted and bystander Air-100 cells. The fraction of unmethylated CCGG sites was determined in the side (bystander cells only; *blue*) and central (bystander and targeted cells; *red*) regions of the tissue at various times after irradiation by comparing cutting by *Hpa*II, a methylation-sensitive restriction enzyme, and *Msp*I, a methylation-insensitive isoschizomer. *Points,* % [^{3}H]dCTP incorporation; *bars,* SD. *B,* SA-β-gal staining of Air-100 and EFT-300 control and bystander tissues. Blue staining indicates SA-β-gal–positive cells. Positive SA-β-gal staining was detected at 3 d after irradiation in bystander Air-100 epithelium and EFT-300 dermal fibroblasts and at 5 d after irradiation in bystander EFT-300 epidermal keratinocytes. *Red arrows,* examples of SA-β-gal–positive fibroblasts, which are difficult to recognize because of their low density. Corresponding proliferation indexes (fractions of PCNA-positive cells) are shown in the top parts of the images.

control mock-irradiated bystander cells (Fig. 5*B*, corresponding proliferation indexes), 4.7-fold lower for AIR-100 and 2.5-fold for EFT-300 keratinocytes. However, no decrease in the incidence of telomere signals in bystander tissues due to telomere shortening was observed, indicating an accelerated telomere-independent nature of the observed senescence (data not shown).

Discussion

In this study, we assessed the kinetics of DSB induction and repair in bystander human tissue models and found more dramatic differences with DSB formation in directly irradiated cells than those observed in cell culture experiments (13–15, 44, 45). In cell culture medium transfer experiments, the levels of γ-H2AX foci in bystander cells were maximal after overnight incubation and decreased by 48 h after irradiation (13), whereas in coculture experiments, where gap junctions are present, the response was higher and the foci remained for at least 48 h, returning to background levels after 72 h (13, 45). Markedly, in tissue models, the level of DSBs reached a plateau by the 1st day after irradiation, stayed elevated for several days, and declined by 6 to 7 days after irradiation. The persistence of elevated DSB levels in the bystander cells and tissues may suggest that they are continuously produced by DNA-damaging agents released from the irradiated cells. However, the disappearance of the majority of γ-H2AX foci by 7 days after irradiation indicates that the cells of these tissues are capable of DSB repair. The increased time required for bystander DSB repair in tissues as opposed to cells in culture indicates increased intensity and persistence in signaling, perhaps due to more physiologic cellular connections in the tissue models. It should be noted that these tissue models exhibit many properties identical to airway epithelium and skin *in vivo*, and the full thickness human skin models are widely used instead of animals for skin testing.

Increased levels of γ-H2AX foci were not uniform but limited to a subset of the bystander cell population, and we therefore speculated that certain phases of the cell cycle might be more sensitive to the transmitted bystander signals (13). Recently, Burdak-Rothkamm et al. (45) reported that the induction of γ-H2AX foci was restricted to bystander cells undergoing replication. However, we found in the tissue models that the fractions of bystander cells exhibiting multiple γ-H2AX foci were much higher than the fractions of PCNA-positive cells in the corresponding sections, indicating that focal induction was not limited to replicating cells. It may be that bystander cells in S phase respond first followed by those in other phases of the cell cycle. Further studies are required to clarify the importance of cell cycle phases in the bystander response.

DNA DSBs in irradiated cells precede the later increases in the levels of apoptosis, micronuclei, DNA hypomethylation, and senescence markers. Bystander DSBs may also be precursors to the global long-term changes. For example, the increased global DNA hypomethylation observed in bystander tissues may result from the increased presence of DNA DSBs and other lesions, which may interfere with the activity of DNA methyltransferases. It has been shown that DNA lesions, such as DNA DSBs, and oxidative base damage may result in hypomethylation (35, 46). Furthermore, the appearance of DNA lesions has been shown to precede hypomethylation of DNA in human lymphocytes (27). A recent report connected radiation-induced DNA damage in bystander tissues *in vivo* with suppression of global DNA methylation and epigenetic transcriptional regulation (8). Thus, the observed hypomethylation in the bystander tissue is very likely to be a result of accumulation and repair of genotoxic lesions in DNA.

Treatment of primary tumors with radiation therapy frequently results in the growth of a secondary malignancy of the same or different origin. An important question concerns the biological role of the bystander effects: are they negative complications in radiation oncology, introducing genomic instability to unirradiated normal tissues, or important protective responses to the homeostasis of the whole organism? Here, we connect the bystander effect with cellular senescence and report that bystander cells of different origins undergo an accelerated senescence at 3 to 5 days after exposure. Some exogenous agents, including irradiation, have been reported to induce premature senescence in normal human cells (47, 48), and we have found previously that DSB-inducing chemicals can cause premature senescence (39). Senescence is a tumor suppressor mechanism (49), which, like apoptosis and DNA DSB repair, has been proposed to be a programmed protective response to potentially carcinogenic cellular changes (50). Possibly, a premature cellular senescence initiated by bystander DNA DSBs around an exposure site also may serve as a protective barrier.

Our study shows for the first time the widespread nature and time-dependent propagation of the bystander response in tissue models. We propose that the bystander effect is a complex response partially or wholly initiated by radiation-induced DSB formation in bystander tissues and involving multiple DNA damage pathways, which may serve as a protective response in the whole organism to ongoing accumulation of DNA lesions. The failure of these protective pathways can lead to the appearance of proliferating, damaged cells and to an increased probability of oncogenic transformation.

Acknowledgments

Received 12/4/2006; revised 1/16/2007; accepted 2/8/2007.

Grant support: Intramural Research Program of the National Cancer Institute, Center for Cancer Research, NIH (O.A. Sedelnikova, A. Nakamura, and W.M. Bonner); National Science and Engineering Council of Canada and Canadian Institutes of Health grants (O. Kovalchuk and I. Koturbash); and U.S. Department of Energy Low Dose Radiation Program grants DE-FG02-03ER63632 and DE-FG02-01ER63226 and NIH grants P41 EB002033-09 and P01 CA-49062 (S.A. Mitchell, S.A. Marino, and D.J. Brenner).

The costs of publication of this article were defrayed in part by the payment of page charges. This article must therefore be hereby marked *advertisement* in accordance with 18 U.S.C. Section 1734 solely to indicate this fact.

We thank the RARAF staff (Columbia University) for help with microbeam irradiation; Lubomir Smilenov (Columbia University) for his continuous support; Igor Panyutin and Jennifer Dickey (NIH) for critical reading of the article; and Robert Statz and Jordan Zaner (NIH) for data entry and statistical analysis.

References

1. Brenner DJ, Little JB, Sachs RK. The bystander effect in radiation oncogenesis: II. A quantitative model. Radiat Res 2001;155:402–8.
2. Bonner WM. Phenomena leading to cell survival values which deviate from linear-quadratic models. Mutat Res 2004;568:33–9.
3. Little JB. Cellular radiation effects and the bystander response. Mutat Res 2006;597:113–8.
4. Hall EJ, Hei TK. Genomic instability and bystander effects induced by high-LET radiation. Oncogene 2003; 22:7034–42.
5. Morgan WF. Non-targeted and delayed effects of exposure to ionizing radiation: I. Radiation-induced genomic instability and bystander effects *in vitro*. Radiat Res 2003;159:567–80.
6. Morgan WF. Non-targeted and delayed effects of exposure to ionizing radiation: II. Radiation-induced genomic instability and bystander effects *in vivo*, clastogenic factors, and transgenerational effects. Radiat Res 2003;159:581–9.
7. Azzam EI, de Toledo SM, Little JB. Stress signaling from irradiated to non-irradiated cells. Curr Cancer Drug Targets 2004;4:53–64.
8. Koturbash I, Rugo RE, Hendricks CA, et al. Irradiation induces DNA damage and modulates epigenetic effectors in distant bystander tissue *in vivo*. Oncogene 2006; 25:4267–75.
9. Kaup S, Grandjean V, Mukkherjee R, et al. Radiation-induced genomic instability is associated with DNA methylation changes in cultured human keratinocytes. Mutat Res 2006;597:87–97.
10. Kashino G, Prise KM, Schettino G, et al. Evidence for induction of DNA double strand breaks in the bystander response to targeted soft X-rays in CHO cells. Mutat Res 2004;556:209–5.
11. Sedelnikova OA, Pilch DR, Redon C, Bonner WM. Histone H2AX in DNA damage and repair. Cancer Biol Ther 2003;2:233–35.
12. Pilch DR, Sedelnikova OA, Redon C, Celeste A, Nussenzweig A, Bonner WM. Characteristics of γ-H2AX foci at DNA double-strand breaks sites. Biochem Cell Biol 2003;81:123–9.
13. Sokolov MV, Smilenov LB, Hall EJ, Panyutin IG, Bonner WM, Sedelnikova OA. Ionizing radiation induces DNA double-strand breaks in bystander primary human fibroblasts. Oncogene 2005;24:7257–65.
14. Yang H, Asaad N, Held KD. Medium-mediated intercellular communication is involved in bystander responses of X-ray-irradiated normal human fibroblasts. Oncogene 2005;24:2096–103.
15. Hu B, Wu L, Han W, et al. The time and spatial effects of bystander response in mammalian cells induced by low dose radiation. Carcinogenesis 2005;27:245–51.
16. Belyakov OV, Folkard M, Mothersill C, Prise KM, Michael BD. Bystander-induced apoptosis and premature differentiation in primary urothelial explants after charged particle microbeam irradiation. Radiat Prot Dosimetry 2002;99:249–51.
17. Belyakov OV, Folkard M, Mothersill C, Prise KM, Michael BD. A proliferation-dependent bystander effect in primary porcine and human urothelial explants in response to targeted irradiation. Br J Cancer 2003;88: 767–74.
18. Belyakov OV, Folkard M, Mothersill C, Prise KM, Michael BD. Bystander-induced differentiation: a major response to targeted irradiation of a urothelial explant model. Mutat Res 2006;597:43–9.
19. Mothersill C, O'Malley K, Seymour CB. Characterisation of a bystander effect induced in human tissue explant cultures by low let radiation. Radiat Prot Dosimetry 2002;99:163–7.
20. Persaud R, Zhou H, Baker SE, Hei TK, Hall EJ. Assessment of low linear energy transfer radiation-induced bystander mutagenesis in a three-dimensional culture model. Cancer Res 2005;65:9876–82.
21. Belyakov OV, Mitchell SA, Parikh D, et al. Biological effects in unirradiated human tissue induced by radiation damage up to 1 mm away. Proc Natl Acad Sci U S A 2005;102:14203–8.
22. Zhao JF, Zhang YJ, Kubilus J, et al. Reconstituted 3-dimensional human skin as a novel *in vitro* model for studies of carcinogenesis. Biochem Biophys Res Commun 1999;254:49–53.
23. Boelsma E, Gibbs S, Faller C, Ponec M. Characterization and comparison of reconstructed skin models: morphological and immunohistochemical evaluation. Acta Derm Venereol 2000;80:82–8.
24. Mothersill C, Seymour C. Radiation-induced bystander effects: are they good, or bad or both? Med Confl Surviv 2005;21:101–10.
25. Randers-Pehrson G, Geard CR, Johnson G, Elliston CD, Brenner DJ. The Columbia University single-ion microbeam. Radiat Res 2001;156:210–4.
26. Rogakou EP, Boon C, Redon C, Bonner WM. Megabase chromatin domains involved in DNA double-strand breaks *in vivo*. J Cell Biol 1999;146:905–15.
27. Pogribny I, Yi P, James SJ. A sensitive new method for rapid detection of abnormal methylation patterns in global DNA and within CpG islands. Biochem Biophys Res Commun 1999;262:624–8.
28. Pogribny I, Koturbash I, Tryndyak V, et al. Fractionated low-dose radiation exposure leads to accumulation of DNA damage and profound alterations in DNA and histone methylation in the murine thymus. Mol Cancer Res 2005;3:553–61.
29. Zhivotovsky B, Samali A, Gahm A, Orrenius S. Caspases: their intracellular localization and translocation during apoptosis. Cell Death Differ 1999;6:644–51.
30. Fenech M. The *in vitro* micronucleus technique. Mutat Res 2000;455:81–95.
31. Thierens H, De Ruyck K, Vral A, et al. Cytogenetic biodosimetry of an accidental exposure of a radiological worker using multiple assays. Radiat Prot Dosimetry 2005;113:408–14.
32. Celeste A, Petersen S, Romanienko PJ, et al. Genomic instability in mice lacking histone H2AX. Science 2002; 296:922–7.
33. Lu C, Zhu F, Cho Y-Y, Tang F, et al. Cell apoptosis: requirement of H2AX in DNA ladder formation, but not for activation of caspase-3. Mol Cell 2006;23: 121–32.
34. Cerda S, Weitzman SA. Influence of oxygen radical injury on DNA methylation. Mutat Res 1997;386:141–52.
35. Pogribny I, Raiche J, Slovack M, Kovalchuk O. Dose-dependence, sex- and tissue-specificity, and persistence of radiation-induced genomic DNA methylation changes. Biochem Biophys Res Commun 2004;320: 1253–61.
36. Pogribny IP, James SJ, Jernigan S, Pogribna M. Genomic hypomethylation is specific for preneoplastic liver in folate/methyl deficient rats and does not occur in non-target tissues. Mutat Res 2004;548:53–9.
37. Raiche J, Rodriguez-Juarez R, Pogribny I, Kovalchuk O. Sex- and tissue-specific expression of maintenance and *de novo* DNA methyltransferases upon low dose X-irradiation in mice. Biochem Biophys Res Commun 2004;325:39–47.
38. Wachsman JT. DNA methylation and the association between genetic and epigenetic changes: relation to carcinogenesis. Mutat Res 1997;375:1–8.
39. Sedelnikova OA, Horikawa I, Zimonjic DB, Popescu NC, Bonner WM, Barrett JC. Senescing human cells and ageing mice accumulate DNA lesions with unrepairable double-strand breaks. Nat Cell Biol 2004;6:168–70.
40. Nilsson O, Mitchum RD, Jr., Schrier L, et al. Growth

plate senescence is associated with loss of DNA methylation. J Endocrinol 2005;186:241–9.
41. Roninson IB, Broude EV, Chang BD. If not apoptosis, then what? Treatment-induced senescence and mitotic catastrophe in tumor cells. Drug Resist Updat 2001;4: 303–13.
42. Wojda A, Witt M. Manifestations of ageing at the cytogenetic level. J Appl Genet 2003;44:383–99.
43. Dimri GP, Lee X, Basile G, et al. A biomarker that identifies senescent human cells in culture and in aging skin *in vivo*. Proc Natl Acad Sci U S A 1995;92:9363–7.
44. Smilenov LB, Hall EJ, Bonner WM, Sedelnikova OA. A microbeam study of DNA double-strand breaks in bystander primary human fibroblasts. Radiat Prot Dosimetry. Epub 2006 Dec 12.
45. Burdak-Rothkamm S, Short Sc, Folkard M, Rothkamm K, Prise KM. ATR-dependent radiation-induced γH2AX foci in bystander primary human astrocytes and glioma cells. Oncogene 2007;26:993–1002.
46. Duthie SJ, Narayanan S, Blum S, Pirie L, Brand GM. Folate deficiency *in vitro* induces uracil misincorporation and DNA hypomethylation and inhibits DNA excision repair in immortalized normal human colon epithelial cells. Nutr Cancer 2000;37:245–51.
47. Robles SJ, Adami GR. Agents that cause DNA double strand breaks lead to p16INK4a enrichment and the premature senescence of normal fibroblasts. Oncogene 1998;16:1113–23.
48. Horikawa I, Yawata T, Barrett JC. Cellular senescence mechanisms independent of telomere shortening and telomerase: other barriers to cell immortalization and carcinogenesis. J Anti Aging Med 2007;26:993–1002.
49. Lynch MD. How does cellular senescence prevent cancer? DNA Cell Biol 2006;25:69–78.
50. Collado M, Gil J, Efeyan A, et al. Tumour biology: senescence in premalignant tumours. Nature 2005;436:642.